TRIBOLOGY TRANSACTIONS
http://dx.doi.org/10.1080/10402004.2016.1206647

stle
Society of Tribologists and Lubrication Engineers

A Finite Element Approach to Modeling Abrasive Wear Modes

Martijn Woldman[a,c], Emile Van Der Heide[a,b], Tiedo Tinga[c], and Marc A. Masen[d]

[a]University of Twente, Enschede, the Netherlands; [b]TNO, Eindhoven, The Netherlands; [c]Netherlands Defence Academy, Den Helder, The Netherlands; [d]Imperial College London, Exhibition Road, London, United Kingdom

ABSTRACT
Machine components operating in sandy environments will wear because of the abrasive interaction with sand particles. In this work, a method is derived to predict the amount of wear caused by such abrasive action, in order to improve the maintenance concept of the components. A finite element model is used to simulate various tips scratching a smooth surface. The model is verified by comparing the obtained results with a set of experiments performed earlier (M. Woldman, et al., 2013, Wear, 301(1–2), pp 76–81).

ARTICLE HISTORY
Received 6 August 2015
Accepted 23 June 2016

KEYWORDS
Abrasive wear; wear modeling; abrasive wear types

Introduction

Abrasive wear of machine components is a problem for equipment operating in sandy environments. The damage inflicted on, for example, plain and roller bearings affects the performance of the machine, reducing maintenance intervals and ultimately leading to failure. In order to optimize the maintenance strategy and prevent failure from arising, it has to be possible to understand and predict the abrasive process. In this work, a model is proposed to predict third-body abrasive wear rates and to help understand the abrasive wear process.

Abrasion is a rather complex process that is influenced by a variety of parameters, ranging from the properties of the contacting materials to the environmental and operating conditions, such as applied loads and relative humidity. In third-body abrasion, the properties of the particles that cause wear have a great influence, according to, for example, Woldman, et al. *(1)*, Stachowiak and Stachowiak *(2)* and Williams *(3)*. The most important particle properties that influence abrasive wear are the size, shape, and hardness. Although substantial research effort has been put into establishing the relationships between these parameters and abrasion (De Pellegrin and Stachowiak *(4)*, *(5)*; De Pellegrin, et al. *(6)*; Gåhlin and Jacobson *(7)*; Hutchings *(8)*; Misra and Finnie *(9)*; Sin, et al. *(10)*; Xie and Bhushan *(11)*; Jourani and Bouvier *(12)*; Zhou, et al. *(13)*), the mechanisms are still not fully understood and more in-depth knowledge is required to be able to define and quantify the relationships in a more general way. One way of doing this is with the help of a numerical model for the interaction between abrading particles and abraded surfaces.

Various papers discuss the application of finite element modeling techniques to study material removal processes (see, e.g., Fang, et al. *(14)*; Jain, et al. *(15)*; Maekawa *(16)*; Tian and Saka *(17)*; Schermann, et al. *(18)*; Mamalis, et al. *(19)*). These models are typically applied to subtractive manufacturing processes such as cutting (Maekawa *(16)*; Schermann, et al. *(18)*) or abrasive flow machining (Jain, et al. *(15)*). In these manufacturing processes, the mechanisms underlying material removal are similar to those encountered during abrasive wear. During the scratching interaction between an abrasive particle and a steel surface, material can by removed by a number of mechanisms (see, e.g., Challen and Oxley *(20)*; Hokkirigawa and Kato *(21)*; Masen, et al. *(22)*, *(23)*). Three main wear regimes can be distinguished that can occur depending on the loading conditions and the geometry of the abrasive particles. Under low loads and with rather blunt particles, the main abrasive regime is ploughing or rubbing and a scratch is formed due to plastic deformation of the material. Most numerical models that describe scratching interaction (see, e.g., Fang, et al. *(14)*; Tian and Saka *(17)*) are limited to describing this regime, utilizing an elastic–plastic stress–strain relation to allow for plastic deformation without actual material removal taking place. Under more severe conditions and with sharper abrasive particles, actual material removal occurs and the contact operates in either the wedge formation or the cutting regime. To include these two regimes in a numerical model, some kind of definition or criterion for material removal is required. This can be done by implementing published work on machining and cutting processes (Maekawa *(16)*; Schermann, et al. *(18)*).

In earlier work by the authors, the influence of particle size and shape on the abrasive wear were studied experimentally (Woldman, et al. *(1)*, *(24)*). More specifically, in Woldman, et al. *(1)*, the influence of particle size on abrasion was studied by performing single asperity scratch tests. Spherical SiO_2 tips with varying radii were used to scratch smooth steel surfaces. In real applications, however, particles will not be spherical but have a more random shape, which has to be taken into account to be able to predict the wear arising to a reasonable extent. In Woldman, et al. *(25)*, particle shape definitions were derived

CONTACT Emile Van Der Heide e.vanderheide@utwente.nl
Color versions of one or more of the figures in the article can be found online at www.tandfonline.com/utrb.
Review led by Al Segall

that quantify the shape of random particles as a deviation of a spherical particle. These findings need to be verified in order to be able to assess the influence of particle shape on abrasive wear, which can be done by numerically modeling the experimental setup used in Woldman, et al. *(1)* and extending this to situations with various tip sizes. In this way, the particle shape effect can be verified and a more general model for the wear caused by the abrasive action of particles can be derived.

This article discusses a finite element model for the ploughing and scratching action of an SiO_2 tip with a predefined radius over a smooth steel surface. By using a selection of tips with their geometry varying from spherical to pyramidal and verifying them with the results from Woldman, et al. *(1)*, the shape parameters from Woldman, et al. *(25)* can be verified and a general model for a ploughing and scratching asperity can be obtained. The setup of the model will be discussed in the following section. Then the model is verified and applied to different tip shapes.

Model definition

The abrasive wear finite element model is developed using Abaqus/Explicit. The explicit option is used to include the plastic deformations and material removal involved in abrasive wear processes. The model consists of a discrete rigid tip and a flat deformable surface. In the simulations the tip is constrained in all directions, and the surface is positioned under the tip and moves so that a groove is formed on the surface.

Tip geometry and properties

The initial model for the abrasive medium is the tip used in the single asperity scratch tests described in Woldman, et al. *(1)*, as shown in Fig. 1. To minimize the number of elements and thereby the computational time, the base of the tip is not modeled entirely. This can be done without introducing errors because only the tip of the indenter is involved in the scratching process, and the base is used for clamping and does not influence the scratching behavior.

The tip material is quartz and Table 1 gives the relevant properties of this material. During abrasive wear the surfaces deform plastically and can be considered nondeformable because the tip is much harder than the steel surface and practically does not wear during the scratching movement. These assumptions reduce the required computation time to solve the numerical model. The reference point for the rigid body, where in Abaqus the possible boundary conditions, loads and displacements, and material properties are applied, is defined as the apex of the tip. Although a rigid body will not deform and therefore the mechanical properties do not have any effect on the calculated results, Abaqus/Explicit requires a mass to be specified. The mass of the tips that were employed in the single asperity scratch tests discussed in Woldman, et al. *(1)* was 18 mg and therefore this value is used in the numerical model. The tip is fully constrained to prevent it from moving during the simulation. The meshing of the tip is kept as coarse as possible to decrease the computational time. The total number of elements on the tip is 1,200, and the approximate element size around the apex is 5 μm.

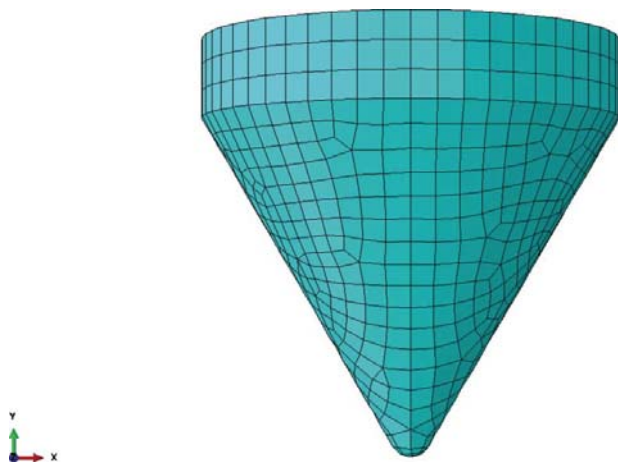

Figure 1. Representation of the tip used in the numerical simulations; spherical $R = 50$ μm.

Table 1. Mechanical properties of the materials tested.

Material	Steel (DIN St-52)	Quartz (SiO_2)
Hardness (GPa)	2	9.8
Young's modulus (GPa)	210	73
Density (kg/m^3)	7,800	2,200
Poisson's ratio	0.30	0.17

Specimen geometry and material behavior

The surface to be scratched is modeled similar to the steel specimens used in the single asperity scratch tests. The specimen material is St. 52, for which the relevant properties are listed in Table 1. The specimen used in Abaqus is shown in Fig. 2a. It is not a representation of the complete specimen as used in the experiments in Woldman, et al. *(1)*; only the region that is influenced by the scratching movement of the tip is included. By applying symmetry boundary conditions to the sides, the rest of the specimen is still taken into account but elements do not need to be appointed. This is done to decrease the total number of elements and thus the computational time. Typical wear grooves in Woldman, et al. *(1)*, resulting from the scratching of a tip with a radius of 50 μm, is up to a few micrometers deep, with a width on the order of several tens of micrometers, and therefore the dimensions of the modeled scratched specimen are $300 \times 200 \times 15$ μm, and the dimensions of the individual elements are 1 μm, which is small enough to ensure that minor changes in the geometry can be simulated.

The material model for the specimen allows for material removal, or wear, to occur in the form of plasticity as well as removal of elements. The plastic material behavior is modeled by extending the linearly elastic part of the stress–strain curve with a plastic part beyond the yield point. In Abaqus this is done by defining tables with values for the stress depending on the plastic strain for various values of the strain rate (see Fig. 3), which has been adapted from Majzoobi, et al. *(26)* for an St. 52 steel alloy similar to the one that was applied in the single asperity scratch tests.

To account for damage under compressive stress conditions, the Johnson-Cook failure model is used (Johnson and Cook *(27)*). With this model, the fracture strain is calculated based

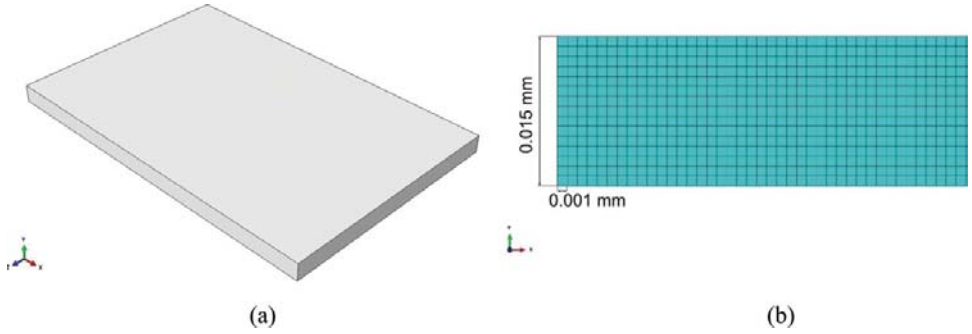

Figure 2. Representation of the specimen used in the numerical simulations (a) with a cross section to show the element size in (b).

on the pressure, strain rate, and temperature. Damage is quantified by the damage parameter D:

$$D = \sum \frac{\Delta\varepsilon}{\varepsilon^f} \quad [1]$$

with $\Delta\varepsilon$ the increment of equivalent plastic strain during an integration cycle and ε^f the equivalent plastic fracture strain (Woldman, et al. *(24)*). Fracture will occur when the equivalent plastic strain equals the fracture strain; that is, the damage parameter D is equal to 1. The fracture strain at room temperature is defined as

$$\varepsilon^f = [D_1 + D_2 \cdot e^{D_3 \cdot \sigma^*}][1 + D_4 \cdot \ln\dot{\varepsilon}^*] \quad [2]$$

in which D_1–D_4 are constant material parameters as obtained empirically for steel by Johnson and Cook *(27)*, as listed in Table 2. The pressure–stress ratio σ^* and the dimensionless strain rate $\dot{\varepsilon}^*$ and $\sigma^* \leq 1.5$ are defined as

$$\sigma^* = \frac{\sigma_m}{\overline{\sigma}}$$
$$\dot{\varepsilon}^* = \frac{\dot{\varepsilon}}{\dot{\varepsilon}_0}, \ with\ \dot{\varepsilon}_0 = 1\ s^{-1} \quad [3]$$

with σ_m the average normal stress, $\overline{\sigma}$ the equivalent von Mises stress, and $\dot{\varepsilon}$ the actual strain rate.

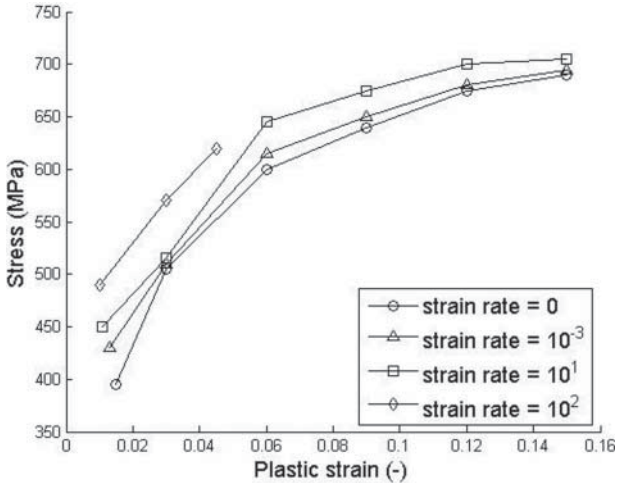

Figure 3. Plastic material behavior of the steel specimen at different strain rates (s^{-1}).

The Johnson-Cook model (Johnson and Cook *(27)*) induces element removal when the strain in an element exceeds the fracture strain as defined in Eq. [2]. This leads to volume loss of the surface and thus to wear of the scratched material.

Though the Johnson-Cook model (Johnson and Cook *(27)*) applies to damage under compressive stress conditions, damage may also be caused by shear stresses acting in the deforming material. Certainly when large deformations arise, local shear bands may form; zones of large shear strains cause damage to the material and ultimately lead to failure. In Abaqus, a shear criterion can be included in the material model to predict the onset of damage due to this formation of shear bands. Referring to Abaqus *(28)*, the equivalent plastic strain at the damage initiation can be calculated as a function of the shear stress ratio and the strain rate. If the incremental increase in the equivalent plastic strain yields the total plastic strain to exceed this limit, failure will take place and the element for which this criterion is met will be removed.

Simulations

As stated in the previous section, the required geometrical features of the model are quite detailed because the radius of the tip and the scratch depth are in the order of micrometers. In order to appropriately describe these features, the element size needs to be of the same order or even smaller.

In simulations performed with Abaqus/Explicit, the critical time increment Δt_{cr} above which the simulation becomes unstable is related to the element size according to

$$\Delta t_{cr} = \frac{l}{c} \quad [4]$$

with l the smallest element length (m) and c the wave speed along an element (m/s):

$$c = \sqrt{\frac{E}{\rho}} \quad [5]$$

with E the Young's modulus (Pa) and ρ the material density (kg/m^3). Describing micrometer-sized changes in the surface

Table 2. Parameter values for the Johnson-Cook model for steel, according to Woldman, et al. *(24)*.

Parameter	Value
D_1	0.05
D_2	3.44
D_3	−2.12
D_4	0.002

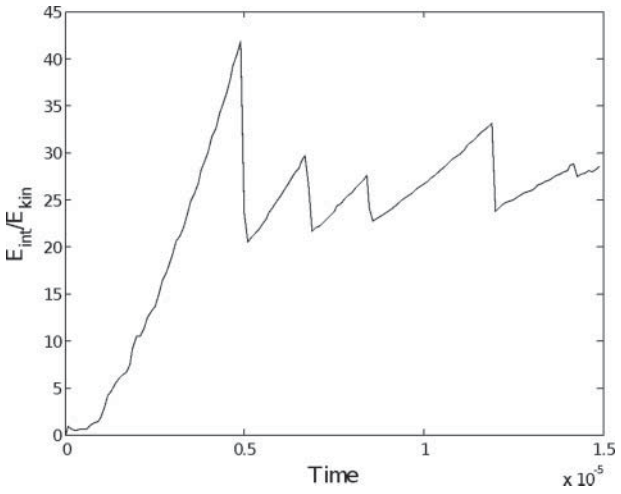

Figure 4. Ratio of internal to kinetic energy in a process depending on the simulation time.

geometry requires a model with very small elements, and according to Eq. [5] these small element sizes induce a small critical time step. In combination with the typically low sliding speeds of the indenter contact (less than 1 mm/s), this means that the calculation times for the simulations become very long, on the order of weeks, even when running the simulations on multiple processors. To speed up the calculation time, some computational tricks may be performed.

Firstly, the calculation time can be decreased by increasing the sliding speed, which is an option when the materials are not strain rate dependent or when the strain rate dependency can be changed in order to account for material behavior at lower speeds. As shown in Fig. 3, in the current situation the material is strain rate dependent and thus the material's strain rate dependencies are artificially changed to account for increased sliding speeds. In practice this means that the *x*-axis of the curves in Fig. 3 is increased to match the range of the sliding speed. Thus, the artificial increase of the sliding speed from 1 to 9,000 mm/s to speed up the calculation requires the strain rates to vary accordingly. A comparison between the results of a slow simulation with the original material stain rate dependencies and a fast simulation with altered material properties indeed did not show any significant differences and hence the computational speeding up is applied in the present work.

Second, mass scaling can be performed to increase the critical time step. As discussed by Olovsson, et al. *(29)*, a higher wave speed results in a larger critical time above which the calculation becomes unstable. This can be achieved by artificially increasing the material density, as long as the kinetic energy in the material remains small compared to the internal energy. Figure 4 shows the ratio of the internal energy and the kinetic energy as a function of the simulation time when the density of the scratched sample is increased 10-fold (from 7,800 to 78,000 kg/m^3). The figure shows that the internal-to–kinetic energy ratio remains large, meaning that the artificially increased density does not influence the simulation results. Artificially changing the strain rate sensitivity and the material density allows an increase in the time step and results in a decrease in the required computation time from around one day to around 3 h.

The single asperity scratch tests described in Woldman, et al. *(1)* are simulated using the described model, using a stationary abrading tip and a moving abraded specimen. An important difference is that the Abaqus/Explicit simulations are performed using displacement-controlled conditions, whereas the experiments were done with a controlled normal load. The reason for this is that load-controlled simulations can cause the stiffness matrix to become singular (De Borst, et al. *(30)*), which is not possible in displacement-controlled simulations; hence, displacement control is used in the simulations described in this article.

Single asperity wear mechanisms

The result of a single asperity scratch test is a groove formed on the specimen by the sliding movement of the tip across the surface, an example of which is shown in Fig. 5.

Based on experiments and inspired by the slip line models of Challen and Oxley *(20)*, Hokkirigawa and Kato *(21)* showed that there are three primary abrasive mechanisms that may occur in the contact between a scratching tip and a scratched surface, with the predominant mechanism depending on the conditions, such as the applied load or the indentation depth, quantified by the degree of penetration, and the friction or the shear strength of the contacting interface between the two materials.

At low loads and thus at low values for the degree of penetration, the tip will plough the surface, forming a groove with a cross section as shown in Fig. 6. In this situation, no actual material loss takes place; rather, the material is pushed downwards and into the shoulders.

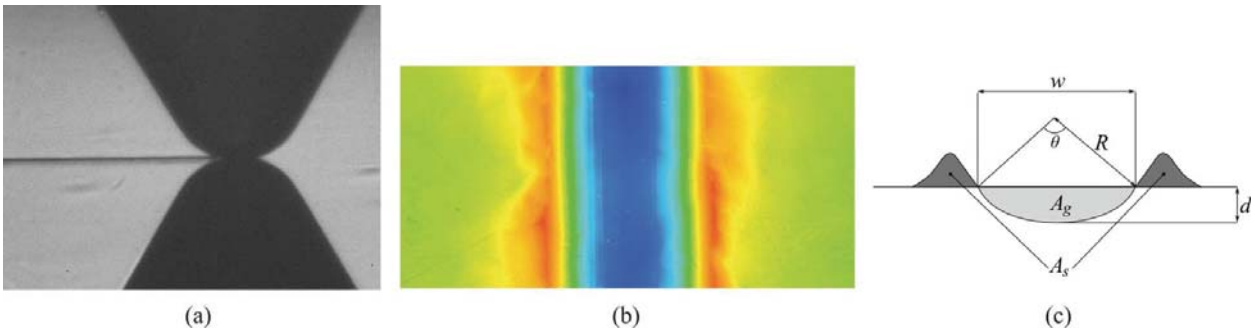

Figure 5. Example of a groove resulting from a single asperity scratch test (a) during the experiment and (b) result of a confocal microscope height profile measurement (blue is low, red is high). (c) Schematic illustration of the cross section of a wear scar.

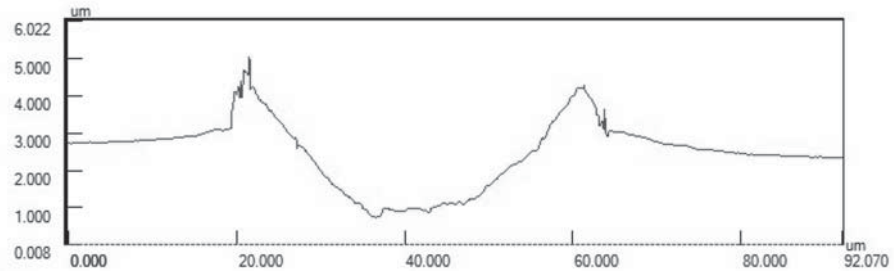

Figure 6. Example of an experimental groove; $R = 100\ \mu$m, $d = 0.002\ \mu$m.

The most severe mechanism of abrasive wear is cutting. In this case almost all material from the groove is removed from the surface in the form of a chip, and no or hardly any shoulders develop along the sides of the groove. In abrasion, this process is typically only observed under extreme conditions, such as high loads and very sharp particles.

Wedge formation is a non-steady-state mechanism that involves a groove being formed and the displaced material from the groove being collected in a "bow" in front of the moving tip. During scratching the bow will grow and ultimately break off (i.e., wear will occur), after which the process of bow initiation and growth restarts.

A scratch and the wear related to the scratching motion can be quantified using the degree of wear parameter, which is a measure for the fraction of the material from the groove that is actually removed from the surface. Referring to the idealized schematic cross section of a wear scar shown in Fig. 5c, the degree of wear β is defined as

$$\beta = \frac{A_g - A_s}{A_g} \quad [6]$$

with A_g the groove area and A_s the shoulder area. A value of β close to 0 means ploughing, whereas a value close of β is indicative of cutting and severe wear.

Hokkirigawa, et al. *(31)* studied the properties of such grooves and showed that the wear is a function of the degree of penetration D_p of the scratching tip into the scratched material, which is defined as

$$D_p = \frac{2d}{w}. \quad [7]$$

Figure 7 shows an adaption of one of the curves presented by Hokkirigawa, et al. *(31)*, showing that the degree of wear increases with increasing degree of penetration following an S-shaped curve. The dotted lines indicate the ploughing, wedging, and cutting wear mechanisms.

The degree of wear parameter is the measure for wear and the degree of penetration quantifies the relative depth of the groove and thus the severity of the contact.

In Woldman, et al. *(1)*, single asperity scratch tests were performed on steel surfaces using quartz tips with predefined radii to study the effects of the indenter size on abrasion. The performed experiments are relatively easy and well controllable; the geometries are prescribed and all system parameters such as applied load and the resulting indentation depth are either known or can be calculated, which enables simulating them in Abaqus. In these single asperity scratch experiments, ploughing was observed for most values of the indentation depth, whereas cutting was only observed at extreme loads and typically resulted in brittle failure of the quartz tips. The aim of the present work is to employ the developed numerical model to reproduce Hokkirigawa, et al.'s *(31)* experimental curve in Fig. 7. A correct reproduction will demonstrate that the model is capable of simulating the three mechanisms for different values of the degree of penetration and friction.

Verification of the model

The numerical model is simulated using the explicit method, which means that the simulations are numerically unconditionally stable. Therefore, the simulation will always complete and produce a result, even when the outcomes are physically not feasible. It is therefore important to verify the results and make sure they are reasonable. In this section the wear as calculated using the numerical model will be studied and a curve similar to the curve shown in Fig. 7 will be obtained. The different wear regimes will be discussed independently.

Ploughing

In Fig. 8, some results are shown for the ploughing situation by plotting the cross section of a simulated groove and its corresponding experimental groove.

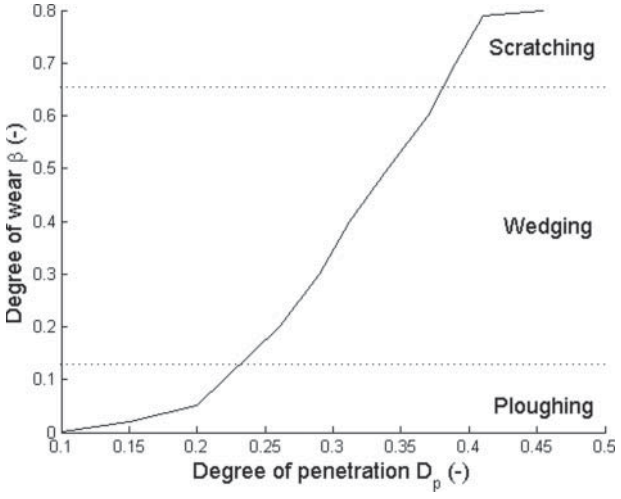

Figure 7. Degree of wear versus degree of penetration. Adapted from Hokkirigawa, et al. *(31)*.

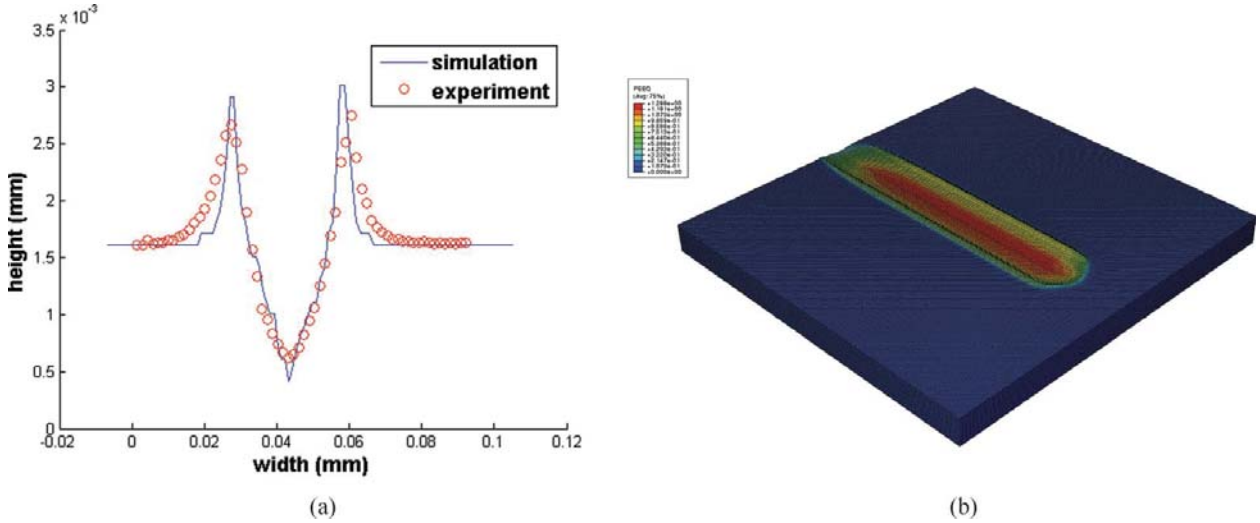

Figure 8. Ploughing results, $R = 50\ \mu$m, $d = 0.001$ mm: (a) cross section and comparison with experiment and (b) overview of the simulated groove.

The results in Fig. 8 indicate that the ploughing behavior of a tip sliding over a surface can be modeled. Ploughing is a predominantly plastic process, without wear or loss of elements in the model. The simulated groove is similar to the experimental groove; both the depth of the groove and the shape of the groove closely resemble each other.

Wedging

For both the wedge formation and cutting mechanisms, actual wear occurs and elements are removed from the mesh. An example of a simulated wedging groove is shown in Fig. 9. The image shows non-steady-state repetitive behavior, showing initiation and growth of the bow. Although the model is capable of modeling the wedge formation mechanism to a reasonable extent, more work is required to improve the modeled material behavior and simulate the correct morphology of the scratch, because the wedge formation is a dynamic, non-steady-state regime where transient effects play an important role.

Cutting

Cutting typically takes place for values of the degree of wear parameter larger than 0.7, resulting in a clear groove with hardly any shoulders. The shear strength of the indenter–surface interface is an important parameter in the onset of the cutting regime, and Challen and Oxley *(20)* showed that a reduction in the shear strength of the interface will result in an earlier onset of cutting. The reduced amount of sticking between the abraded material and the tip prevents the build-up of the bow and facilitates the formation of a freely moving chip. By reducing the coefficient of friction in the model from 0.1 to 0.01, a transition from wedge formation to the cutting regime is obtained in the simulation. This is shown in Fig. 10, where, after a start-up phase, a groove without shoulders, as is typical for cutting, can be observed. It can therefore be concluded that the cutting mechanism can also be simulated and the technique for element removal can be implemented to model the wear regimes.

Application of the model to conical tips

Hokkirigawa, et al. *(31)* quantified abrasive wear by plotting the degree of wear as a function of the depth of indentation into the scratched material. A similar plot can now be produced based on the calculation outcomes of the developed model for the indenter with a radius of 50 μm, as presented earlier. This graph is shown in Fig. 11. Indeed, an approximate S-shaped curve can be observed, and regions for ploughing wedging and cutting can be distinguished.

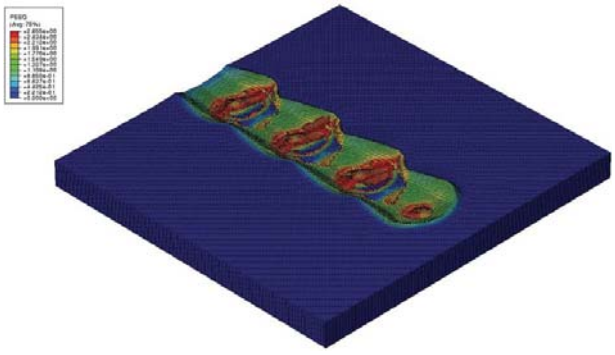

Figure 9. Overview of a wedging groove; $R = 50\ \mu$m, $h = 0.002$ mm.

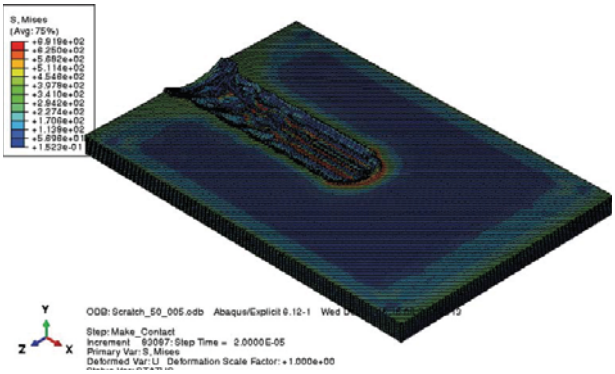

Figure 10. Example of a groove created by cutting.

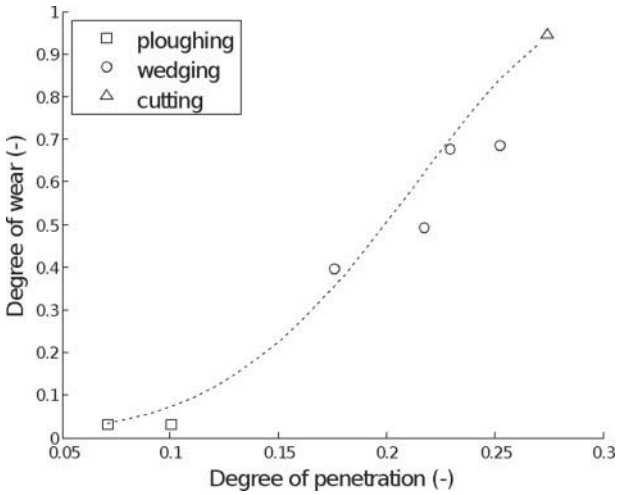

Figure 11. Simulation results; degree of wear plotted against the indentation depth.

Discussion

In the above it has been shown that a relatively simple and straightforward numerical method using finite element modeling can be used to reproduce experimental data on the three typical abrasive wear regimes: ploughing, wedging, and scratching. This indicates that fairly basic numerical methods can be applied to predict abrasive wear. The model can be used to study the effects of 3D particle shape and it provides a basis for future work, wherein topics such as particle orientation and the effects of multiple particles and multiple scratches can be studied in more detail. As an example, the newly developed model could be applied to incorporate the superposition method proposed by da Silva, et al. *(32)*. For such cases, initial validation can be done using literature data; for example, the wear map developed by Xie and Williams *(33)* and results of multipass dual-indenter scratch tests (see, e.g., Xu, et al. *(34)*). The main contribution of this article is the proposed numerical method used for predicting these abrasive wear modes and the verification of the basic principles by comparison with experimental results. The model presented in this article hence provides a solid platform for future investigations and for a more comprehensive approach to abrasive wear modeling.

Conclusions

A relatively straightforward numerical model was developed for the contact of a scratching rigid tip with a predefined shape over a softer, deforming surface. The model provides a basis on which other phenomena such as irregularly shaped particles and multiple-particle and repetitive situations can be implemented. Volumetric wear is included by employing removal of elements using a shear damage criterion based on both fracture strains and equivalent plastic displacement. The model has been verified by reproducing experimental results on the abrasive behavior of a tip sliding over a surface. The three abrasive wear regimes that have been observed in experiments, ploughing, wedging, and scratching, were observed with the model by varying the indentation depth of the tip and the friction characteristics between the tip and the surface; the relationship between indentation depth and material removal as calculated using the model re-creates the characteristic S-shape curve as presented by Hokkirigawa, et al. *(31)*.

References

(1) Woldman, M., Van Der Heide, E., Tinga, T., and Masen, M. A. (2013), "The Influence of Abrasive Body Dimensions on Single Asperity Wear," *Wear*, **301**(1–2), pp 76–81.

(2) Stachowiak, G. B. and Stachowiak, G. W. (2001), "The Effects of Particle Characteristics on Three-Body Abrasive Wear," *Wear*, **249**(3–4), pp 201–207.

(3) Williams, J. (2005), *Engineering Tribology*, Cambridge University Press: Cambridge, UK.

(4) De Pellegrin, D. V. and Stachowiak, G. W. (2002), "Assessing the Role of Particle Shape and Scale in Abrasion Using 'sharpness Analysis': Part I. Technique Development," *Wear*, **253**(9–10), pp 1016–1025.

(5) De Pellegrin, D. V. and Stachowiak, G. W. (2005), "Simulation of Three-Dimensional Abrasive Particles," *Wear*, **258**(1–4), pp 208–216.

(6) De Pellegrin, D. V., Torrance, A. A., and Haran, E. (2009), "Wear Mechanisms and Scale Effects in Two-Body Abrasion," *Wear*, **266**(1–2), pp 13–20.

(7) Gåhlin, R. and Jacobson, S. (1999), "The Particle Size Effect in Abrasion Studied by Controlled Abrasive Surfaces," *Wear*, **224**(1), pp 118–125.

(8) Hutchings, I. M. (1992), *Tribology: Friction and Wear of Engineering Materials*, Edward Arnold: London.

(9) Misra, A. and Finnie, I. (1981), "On the Size Effect in Abrasive and Erosive Wear," *Wear*, **65**(3), pp 359–373.

(10) Sin, H., Saka, N., and Suh, N. P. (1979), "Abrasive Wear Mechanisms and the Grit Size Effect," *Wear*, **55**(1), pp 163–190.

(11) Xie, Y. and Bhushan, B. (1996), "Fundamental Wear Studies with Magnetic Particles and Head Cleaning Agents Used in Magnetic Tapes," *Wear*, **202**(1), pp 3–16.

(12) Jourani, A. and Bouvier, S. (2015), "Friction and Wear Mechanisms of 316L Stainless Steel in Dry Sliding Contact: Effect of Abrasive Particle Size," *Tribology Transactions*, **58**(1), pp 131–139.

(13) Zhou, C., Shan, L., Hight, J. R., Danyluk, S., Ng, S. H., and Pazkowski, A. J. (2011), "Influence of Colloidal Abrasive Size on Material Removal Rate and Surface Finish in SiO_2 Chemical Mechanical Polishing," *Tribology Transactions*, **45**(2), pp 232–238.

(14) Fang, L., Cen, Q. H., Sun, K., Liu, W. M., Zhang, X. F., and Huang, Z. F. (2005), "FEM Computation of Groove Ridge and Monte Carlo Simulation in Two-Body Abrasive Wear," *Wear*, **258**(1–4), pp 265–274.

(15) Jain, R. K., Jain, V. K., and Dixit, P. M. (1999), "Modeling of Material Removal and Surface Roughness in Abrasive Flow Machining Process," *International Journal of Machine Tools and Manufacturing*, **39**(12), pp 1903–1923.

(16) Maekawa, K. (1998), "Computational Aspects of Tribology in Metal Machining," *Proceedings of the Institution of Mechanical Engineers - Part J: Journal of Engineering Tribology*, **212**(4), pp 307–318.

(17) Tian, H. and Saka, N. (1991), "Finite Element Analysis of an Elastic–Plastic Two-Layer Half-Space: Sliding Contact," *Wear*, **148**(2), pp 261–285.

(18) Schermann, T., Marsolek, J., Schmidt, C., and Fleischer, J. (2006), "Aspects of the Simulation of a Cutting Process with ABAQUS/Explicit including the Interaction between the Cutting Process and the Dynamic Behavior of the Machine Tool," Proceedings of the 9th CIRP International Workshop on Modeling of Machining Operations, May 11–12, 2006, Bled, Slovenia.

(19) Mamalis, A. G., Vortselas, A. K., and Panagopoulos, C. N. (2013), "Analytical and Numerical Wear Modeling of Metallic Interfaces: A Statistical Asperity Approach," *Tribology Transactions*, **56**(1), pp 121–129.

(20) Challen, J. M. and Oxley, P. L. B. (1979), "An Explanation of the Different Regimes of Friction and Wear Using Asperity Deformation Models," *Wear*, **53**(2), pp 229–243.
(21) Hokkirigawa, K. and Kato, K. (1988), "An Experimental and Theoretical Investigation of Ploughing, Cutting and Wedge Formation during Abrasive Wear," *Tribology International*, **21**(1), pp 51–57.
(22) Masen, M. A., De Rooij, M. B., and Schipper, D. J. (2005), "Micro-Contact Based Modelling of Abrasive Wear," *Wear*, **258**(1–4), pp 339–348.
(23) Masen, M. A., De Rooij, M. B., Schipper, D. J., Adachi, K., and Kato, K. (2007), "Single Asperity Abrasion of Coated Nodular Cast Iron," *Tribology International*, **40**(2), pp 170–179.
(24) Woldman, M., Van Der Heide, E., Schipper, D. J., Tinga, T., and Masen, M. A. (2012), "Investigating the Influence of Sand Particle Properties on Abrasive Wear Behaviour," *Wear*, **294–295**, pp 419–426.
(25) Woldman, M., Van Der Heide, E., Tinga, T., and Masen, M. A. (2013), "Classification of Particle Shapes in 3D," *Journal of Mechanical Science and Technology*.
(26) Majzoobi, G. H., Freshteh-Saniee, F., Faraj Zadeh Khosroshahi, F., and Beik Mohammadloo, H. (2010), "Determination of Materials Parameters under Dynamic Loading. Part I: Experiments and Simulations," *Computational Materials Science*, **49**(2), pp 192–200.
(27) Johnson, G. R. and Cook, W. H. (1985), "Fracture Characteristics of Three Metals Subjected to Various Strains, Strain Rates, Temperatures and Pressures," *Engineering Fracture Mechanics*, **21**(1), pp 31–48.
(28) Abaqus. (2011), *Analysis User's Manual*.
(29) Olovsson, L., Simonsson, K., and Unosson, M. (2005), "Selective Mass Scaling for Explicit Finite Element Analyses," *International Journal of Numerical Methods in Engineering*, **63**(10), pp 1436–1445.
(30) De Borst, R., Crisfield, M. A., Remmers, J. J. C., and Verhoosel, C. V. (2012), *Nonlinear Finite Element Analysis of Solids and Structures*, West Sussex, UK: John Wiley & Sons Ltd.
(31) Hokkirigawa, K., Kato, K., and Li, Z. Z. (1988), "The Effect of Hardness on the Transition of the Abrasive Wear Mechanism of Steels," *Wear*, **123**(2), pp 241–251.
(32) Da Silva, W. M., Costa, H. L., and De Mello, J. D. B. (2011), "Transitions in Abrasive Wear Mechanisms: Effect of the Superimposition of Interactions," *Wear*, **271**, pp 977–986.
(33) Xie, Y. and Williams, J. A. (1993), "The Generation of Worn Surfaces by the Repeated Interaction of Parallel Grooves," *Wear*, **164**, pp 864–872.
(34) Xu, X., Van Der Zwaag, S., and Xu, W. (2015), "A Novel Multi-Pass Dual-Indenter Scratch Test to Unravel Abrasion Damage Formation in Construction Steels," *Wear*, **322–323**, pp 51–60.